Article

Dimensionless Characterization to Estimate Horizontal Groundwater Velocity from Temperature–Depth Profiles in Aquifers

José Antonio Jiménez-Valera [1],[*] and Francisco Alhama [2]

[1] Mining and Civil Engineering Department, Technical University of Cartagena, 30203 Cartagena, Spain
[2] Applied Physics Department, Technical University of Cartagena, 30203 Cartagena, Spain; paco.alhama@upct.es
[*] Correspondence: jose.jvalera@upct.es

Abstract: The outcome of a dimensionless characterization study in a two-dimensional porous media domain in which groundwater flows at a constant horizontal velocity is presented in this report. Using spatial discrimination, the dimensionless groups that govern the solution patterns are determined from dimensionless governing equations. As a boundary condition on the surface, the case of constant temperature is studied. From the mathematical deduction of the groups, a characteristic horizontal length emerges. This length determines the region in which temperature–depth profiles are affected by flow. Existing analytical solutions have been shown to be invalid due to the severe assumption that the horizontal thermal gradient has a constant value. Therefore, universal solutions based on pi theorem have been obtained for the characteristic horizontal length, temperature field, temperature–depth profiles and horizontal temperature profiles. Dependencies between dimensionless groups have been depicted by universal curves, abacuses and surfaces. These graphical solutions are used in an easy way to estimate groundwater velocity from experimental temperature measurements in the form of an inverse problem. In addition, an easy and fast protocol for estimating fluid flow velocity and groundwater inlet temperature from temperature profile measurements is proposed. This protocol is applied in a scenario of groundwater discharge from a quaternary aquifer to a salty lagoon located in the southeast of Spain.

1. Introduction

The study of the temperature field (temperature patterns) or its dimensionless form coming from the heat balance in semiconfined aquifers with horizontal water flow velocity is a complex problem due to the large number of geometrical and physical parameters involved. However, it is a problem of great interest since this field depends on water velocity that could be derived through experimental measurements of temperature–depth profiles in the form of an inverse problem, avoiding the costly installation of flow meters [1]. The increase in temperature with increased depth in the Earth, known as the geothermal gradient, is not uniform around the globe as this temperature rises in a range of 2–3 °C per 100 m of depth on average [2]. There are many numerical methods for related studies, such as the finite element method, which can provide a general analysis [3], and the boundary element method, which allows for more accurate calculation [4]. Numerical methods cannot quantify transfer in porous media as sufficiently as analytical methods.

Therefore, the fractal theory is well-accepted for analytical analysis of porous media, because it can treat complicated geometry in porous media with higher precision [5,6]. The relationship between temperature–depth profiles and water velocity has been studied by many authors, some of them providing empirical or semiempirical models [7–15].

Suzuki [7] was the first author who proposed a solution in semiconfined aquifers with constant vertical water flow. His solution, later rearranged by Stallman [8], introduced two empirical constants with no clear physical meaning. Lapham [1] presented steady-state and transient solutions based on finite-differences methods, applying them to real scenarios in the United States. Taniguchi [11], based on the work of Stallman [13], provided a new set of universal curves that allows direct estimation of vertical groundwater fluxes in relatively shallow aquifers. Ziagos and Blackwell [10] presented analytical studies for horizontal flow through a thin, permeable layer located between two impermeable regions. Lu and Ge [12] proposed analytical solutions for horizontal and vertical fluid flow under the severe assumption of constant horizontal temperature gradients. Kulongoski and Izbicki [14] proposed an inverse problem that characterizes the physical properties of sediments as well as regions (points) to implement artificial recharges. Finally, Duque et al. [15] estimated the vertical upward velocity in a groundwater–surface water interaction scenario (Ringkøbing Fjord, a coastal lagoon on the west coast of Denmark) using the solution of Bredehoeft and Papadopulos [9], for which a steady state had been reached. Temperature–depth profiles were taken very close to the bed of the coastal lagoon. In relation to two-dimensional problems, many authors try to investigate from a qualitative point of view the flow of water from temperature profiles [16–18]. Apart from the old work of Stallman [8], Cartwright [19] is the only author who studies in a qualitative way the thermal profiles derived from the existence of a horizontal water flow in a shallow semiconfined aquifer. However, his solution assumes the severe assumption of a constant horizontal thermal gradient along the aquifer. Actually, such a gradient emerges in the entrance region where a lineal temperature profile develops. Beyond this region, the vertical temperature profile is lineal and does not depend on water velocity.

Regardless of the temperature boundary conditions at the surface and at the bottom of the aquifer, the existence of horizontal flow with a given inlet temperature different from the others gives rise to a balance of advective and diffusive heat fluxes, determining a steady-state temperature field in a limited region of the aquifer. The characteristic horizontal length is defined as the extent of the developed region of this profile. Our interest in this work is to study temperature–depth profiles within the characteristic length in which the influence of the water velocity can be appreciated and to search for the dimensionless groups that rule the temperature profiles and look for simplified hypotheses that allow obtaining universal solutions [20]. Pi theorem [21] allows us to express these unknowns (characteristic length, temperature profiles, temperatures field, etc.), written in their dimensionless form, as a function of the dimensionless groups [22]. Once it has been verified that the set of dimensionless groups correctly determine the problem, the precise dependence between them is graphically adjusted through numerical simulations. As in many other recent works [23,24], dimensionless groups are formally derived from the dimensionless mathematical model which, in turn, is deduced by introducing dependent and independent, dimensionless and normalized variables (discriminated dimensional analysis). Using spatial discrimination ensures that the references used to set dimensionless variables are different according to each spatial direction while normalization confines the range of values of the variables to interval [0, 1]. Once the dimensionless groups of the problem have been established, they are verified by means of a set of cases in which it is proved that the dimensionless temperature patterns are identical for the same values of the dimensionless groups. Based on these results, a protocol is proposed to solve the inverse problem of estimating water velocity from experimental measurements.

2. Physical, Mathematical and Network Models

Figure 1 shows the physical scheme of the problem as well as temperature and flow boundary conditions in the saturated aquifer. Water penetrates at the left vertical boundary. The upper and lower horizontal surfaces are no-flow conditions. As regards temperature, surface, bottom and left boundaries are first class conditions (Diritlech). The aquifer is large enough to satisfy the temperature profile being completely developed before the right limit, and in order to ensure that water leaves the aquifer with a temperature at the right boundary, a free condition (temperature at this edge does not affect temperatures within the domain) is imposed there. The origin of the domain is shown in Figure 1. The study area is delimited by the length L, a region in which the groundwater velocity has a single horizontal component of constant value.
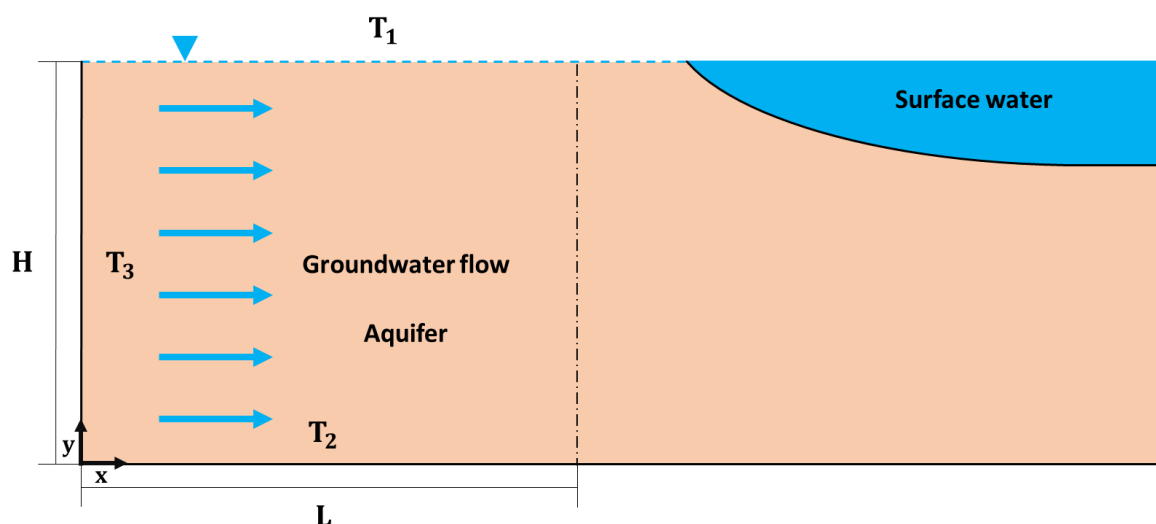

Figure 1. Physical scheme of the problem and boundary conditions.

The velocity field is known, $v(x,y) = v_{x,o}$. Thus, the governing equation is reduced to the expression for heat conservation, resulting from the local balance between diffusion, $\mathbf{j_d} = k \cdot \nabla T$ (Fourier), advection, $\mathbf{j_c} = \rho_{e,w} c_{e,w} \mathbf{v}.\nabla T$ and storage $\mathbf{j_s} = \rho_e c_e \frac{\partial T}{\partial t}$ terms. The equation for the simultaneous flow of fluid and heat on Earth [7] is the governing equation:

$$\rho_e c_e \frac{\partial T}{\partial t} - k\nabla^2(T) + \rho_{e,w} c_{e,w} \mathbf{v}.\nabla(T) = 0 \tag{1}$$

In homogeneous, isotropic domains and rectangular geometry, Equation (1) is written as

$$k\left(\frac{\partial^2 T}{\partial x^2} + \frac{\partial^2 T}{\partial y^2}\right) - \rho_{e,w} c_{e,w} \left(v_{x,o} \frac{\partial T}{\partial x}\right) = \rho_e c_e \frac{\partial T}{\partial t} \tag{2}$$

The equations that establish the initial and boundary conditions complete the mathematical model. These are:

$$T_{(x,y=H,t)} = T_1 \tag{3}$$

$$T_{(x,y=0,t)} = T_2 \tag{4}$$

$$T_{(x=0,y,t)} = T_3 \tag{5}$$

$$\left.\frac{\partial T}{\partial x}\right|_{x=L} = 0 \tag{6}$$

Although it is not relevant for a steady-state solution, the initial temperature (T_{ini}) is assumed in the entire domain to simulate both transient and steady-state solutions. The mathematical model is simulated numerically using the free software Ngspice through a precise model based on the Network Simulation Method [25], a tool that has proven to be effective and reliable in many other problems of similar or greater complexity [26].

The "Network Simulation Method" has been used to carry out the numerical simulations necessary for the construction of universal curves. Instead of using commercial software, this numerical tool (computationally fast) has been chosen thanks to its ease of handling. The Network Simulation Method is a tool that allows the study of any process that can be determined by space-time partial derivative equations to which initial and boundary conditions must be added. The application of the method consists of two phases: first, elaboration of a network model and, second, simulation of the physical process by means of an appropriate electrical circuits software (NgSpice) that allows obtaining the solution of the network model [25]. For the elaboration of a network model, the space must be reticulated in elementary volume elements or cells. Differential equations (in finite differences) are applied to the elements, and the correspondence between variables of the physical problem and those of the network model is established. In this particular case, the electric current corresponds to the groundwater velocity and voltage to the temperature.

Parameters that remain constant are defined: thermal conductivity, specific heats of water and of the water–soil matrix, geometry of the aquifer and horizontal groundwater velocity. For the largest number of simulations carried out, the number of cells was 200 columns and 40 rows (8000 cells in total). The electrical circuit elements within the cells, as well as the electrical elements in the boundary conditions cells, are reflected in Figure 2. The network model will be composed of resistors, capacitors, batteries and voltage generators.
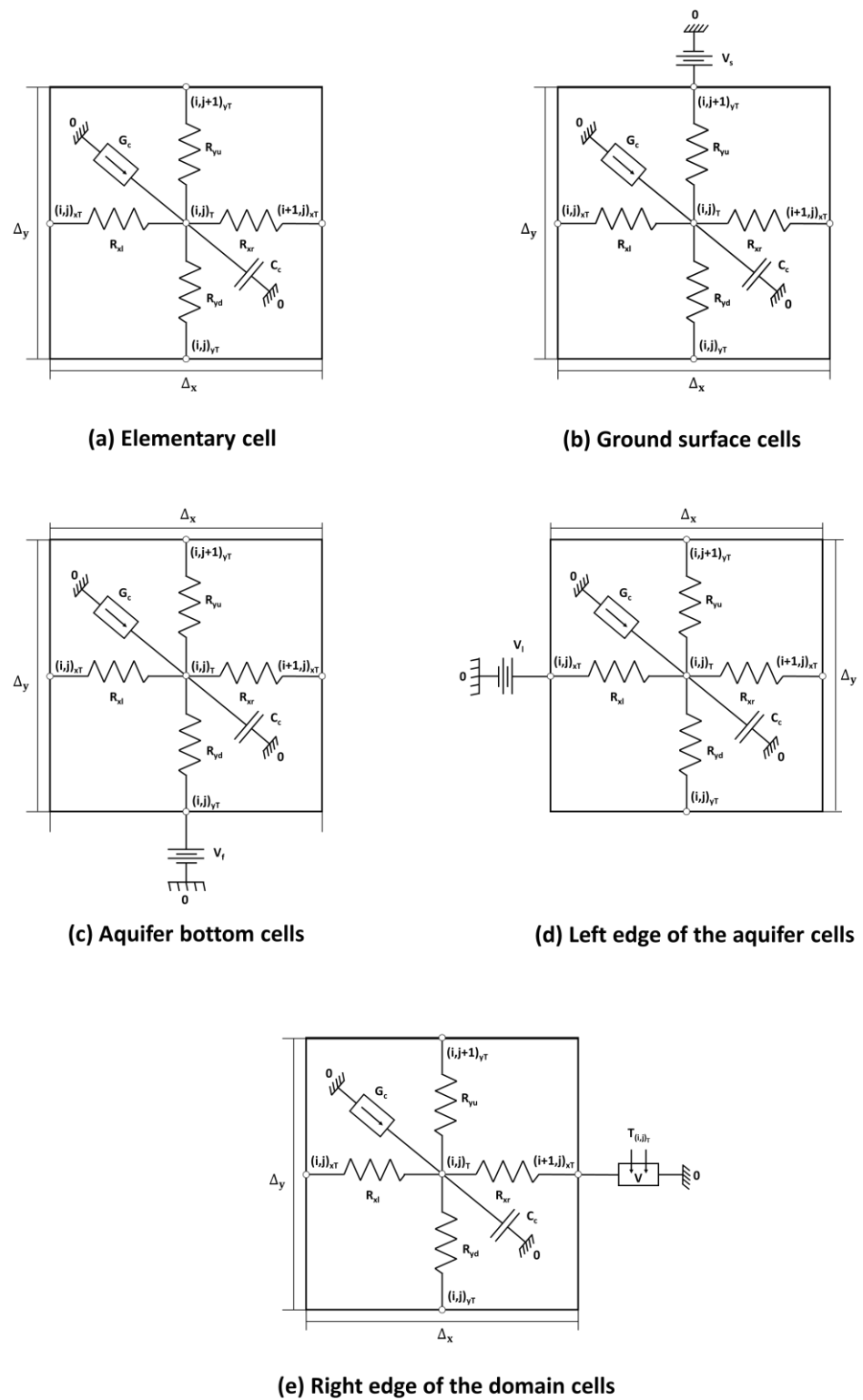
Figure 2. Network models in elementary cell (**a**), cells of the ground surface (**b**), bottom of the domain (**c**), water inlet edge (**d**) and right edge of the domain (**e**).

Spatial discretization of the governing equation for horizontal flow is:

$$k\left[\frac{1}{\Delta x}\left(\frac{\Delta T}{\Delta x}\Big|_{x+} - \frac{\Delta T}{\Delta x}\Big|_{x-}\right)\right] + k\left[\frac{1}{\Delta y}\left(\frac{\Delta T}{\Delta y}\Big|_{y+} - \frac{\Delta T}{\Delta y}\Big|_{y-}\right)\right] - \left(c_{e,w}\rho_{e,w}v_{x,o}\frac{\Delta T}{\Delta x}\right) - (c_e\rho_e)\frac{dT}{dt} = 0 \quad (7)$$

On the other hand, finite difference equation is:

$$\frac{(T)_{i+\frac{\Delta x}{2},j} - (T)_{i,j}}{\frac{(\Delta x)^2}{2k_{m,x}}} + \frac{(T)_{i,j} - (T)_{i-\frac{\Delta x}{2},j}}{\frac{(\Delta x)^2}{2k_{m,x}}} + \frac{(T)_{i,j+\frac{\Delta y}{2}} - (T)_{i,j}}{\frac{(\Delta y)^2}{2k_{m,y}}} + \frac{(T)_{i,j} - (T)_{i,j-\frac{\Delta y}{2}}}{\frac{(\Delta y)^2}{2k_{m,y}}}$$
$$- \rho_{e,w}c_{e.w}v_{x,o}\frac{(T)_{i+\frac{\Delta x}{2},j} - (T)_{i+\frac{\Delta x}{2},j}}{\Delta x} - (\rho_e c_e)\frac{dT_{i,j}}{dt} = 0 \tag{8}$$

Each addend of Equation (9) can be considered as an electric current, which balance each other at the central node of the volume element. From (9), expressions of each parameter of the circuit elements are obtained:

$$R_{xl} = R_{xr} = \frac{(\Delta x)^2}{2 \cdot k_{m,x}} \tag{9}$$

$$R_{yu} = R_{yd} = \frac{(\Delta y)^2}{2 \cdot k_{m,y}} \tag{10}$$

$$G_c = \rho_{e,w}c_{e,w}\frac{v_{x,o}V((i,j)_{xT}, (i+1,j)_{xT})}{\Delta x} \tag{11}$$

The initial temperature of each volume element is set in the capacitors. The batteries located in the cells on the ground surface and in the cells at the bottom of the domain, as well as the cells on the left border (groundwater inflow), will generate a constant value voltage throughout the simulation. These voltages implement the Diritlech condition (constant temperature) at the boundaries.

3. Preliminary Discussion

Regarding the steady-state temperature field, by way of illustration, Figure 3 shows the solution patterns for four typical scenarios whose parameters are listed in Table 1. The temperature at the soil surface is constant for all of them, and, for simplicity, simple values are chosen for lengths and temperatures. These patterns confirm the more relevant aspects of the solution, such as the appearance of a characteristic length (for steady-state solutions in sufficiently extensive scenarios) in which the temperature–depth profiles depend, among other parameters, on groundwater flow velocity. The precise definition of this characteristic length will be established later. Beyond this length, on the one hand, the temperature profiles $(T - y)$ are lineal, independent on time and water velocity. If this length is named $l_{x,T}^*$, temperature–depth profiles develop at $x < l_{x,T}^*$, and bend progressively more the smaller x is compared to $l_{x,T}^*$, that is, they bend as they approach the left edge of the groundwater inlet. On the other hand, the relative value of T_3 compared to T_1 and T_2 determines the existence (or not) of inflections in temperature profiles within a small region close to the left boundary, seeming to weakly influence the value of the characteristic length. As will be seen later, in this small region, the diffusive and advective horizontal effects are comparable. It can be seen that inflections at the profiles emerge when T_3 is within $[T_2, T_1]$ (see Figure 3).
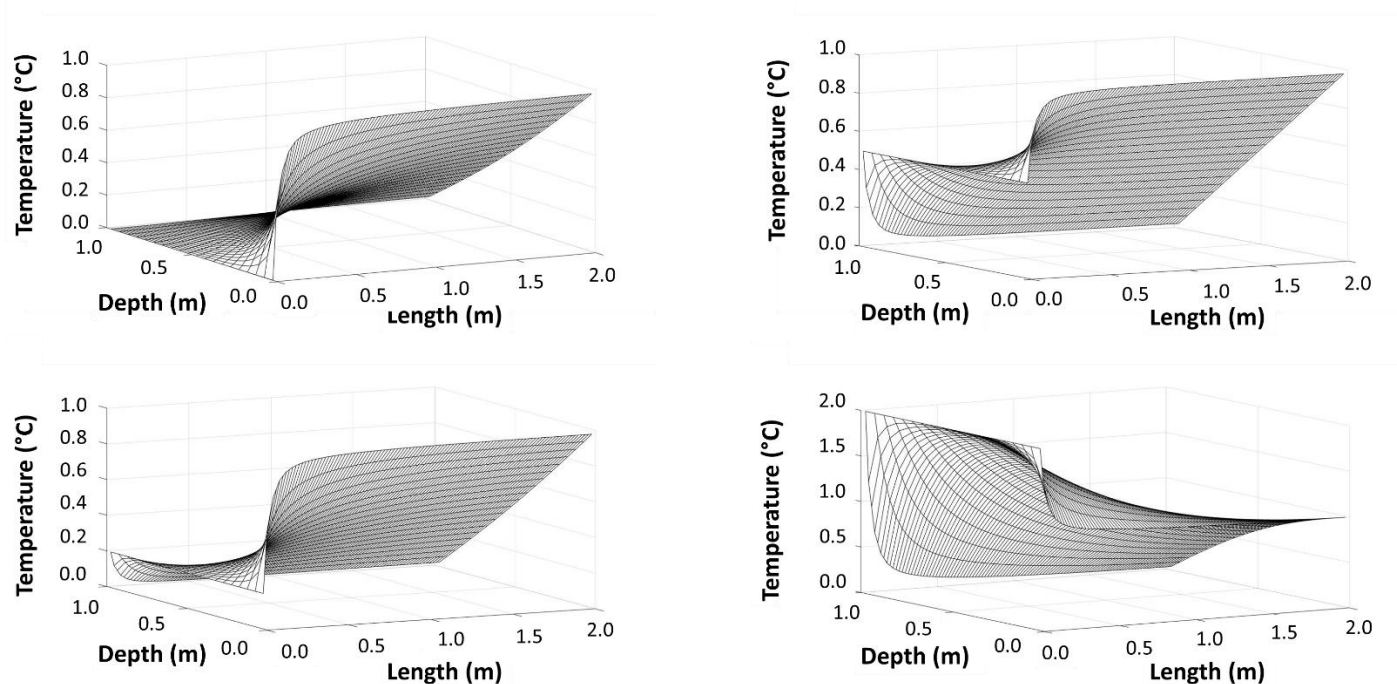
Figure 3. Patterns of the steady-state solution for scenarios of Table 1. Scenarios I and II (**up**) and Scenarios III and IV (**down**).

In real aquifers, with depths of several meters and greater, the horizontal characteristic length increases with the square of the thickness of the aquifer. This dependence will be derived later.

Vertical profiles of temperature at x = 2 m are shown in Figure 4 for these four scenarios. According to these results, while the profile is almost lineal for Scenario II, Scenario III provides a clearly bent profile with a weak inflection at a point closer to the surface due to $|T_3 - T_1| < |T_2 - T_1|$. In Scenario I, curvature of the temperature profile is even more noticeable, and the inflection has disappeared because $T_3 = T_1$. Finally, Scenario IV shows a pronounced curvature with different concavity and no bending, since T_3 is out of the range $[T_1, T_2]$.
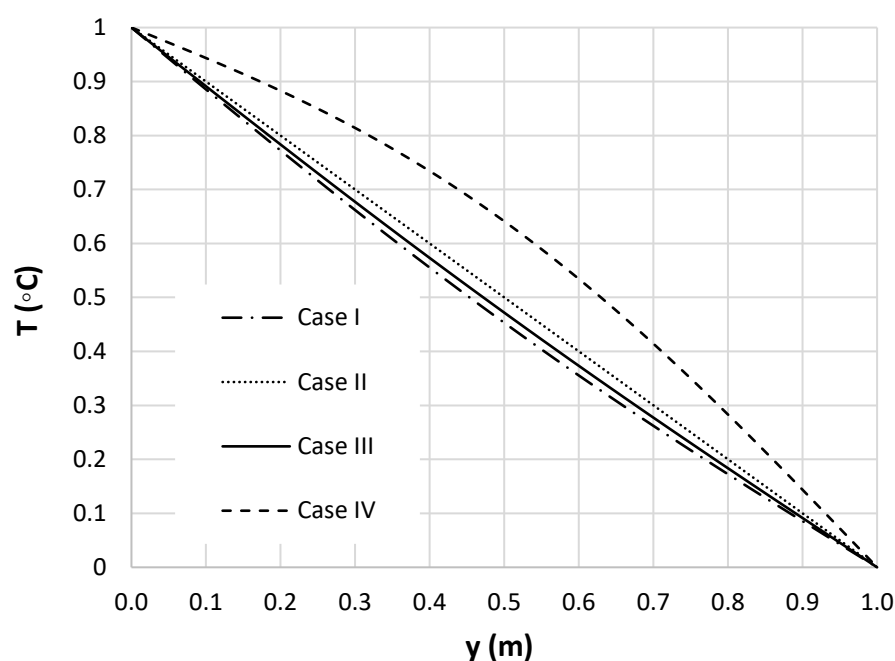
Figure 4. Temperature profiles at x = 2 m for scenarios of Table 1.

Table 1. Parameters of typical scenarios whose patterns are shown in Figure 3.

Scenario	T_1 (°C)	T_3 (°C)	T_2 (°C)	k (cal s⁻¹ m⁻¹ °C⁻¹)	$\rho_e c_e$ (cal/(m³ °C)	$\rho_{e,w} c_{e,w}$ (cal/(m³ °C)	H (m)	$v_{x,o}$ (m/s)
I	0	0	1	0.8	10^6	10^6	1	$5 \cdot 10^{-6}$
II	0	0.5	1	0.8	10^6	10^6	1	$5 \cdot 10^{-6}$
III	0	0.2	1	0.8	10^6	10^6	1	$5 \cdot 10^{-6}$
IV	0	2	1	0.8	10^6	10^6	1	$5 \cdot 10^{-6}$

Continuing with the aim of illustration, Figure 5 shows the horizontal temperature profiles of Scenarios I and III at five depths, $y = \frac{H}{6}, \frac{2H}{6}, \frac{3H}{6}, \frac{4H}{6}$ and $\frac{5H}{6}$. To ensure that $l^*_{x,T} <$ L, L = 10 m has been used in the simulations in this section, although some figures cut this length for a better graphical representation of the region where the temperature profiles develop. It is observed that, although the profiles are less steep near the surface, the temperature ranges in which they move are also of lesser value.

Based on these results and assuming that the aquifers are extensive enough, in the sense that the horizontal diffusive effects are negligible with respect to advective effects, $l^*_{x,T}$ would be defined as the extension of the aquifer from which the dimensionless temperature at the center line of the aquifer (y = H/2) reaches a significant percentage (95–99%) of its steady-state value, $(T_1 + T_2)/2$. From Figure 5, for Scenario III with $(T_1 + T_2)/2 = 0.5$, the characteristic lengths related to percentages 95 and 99% are:

$$T = 0.95 \cdot 0.5 = 0.475 \,°C, \quad l^*_{x,T \, (95\%)} = 2.1 m$$

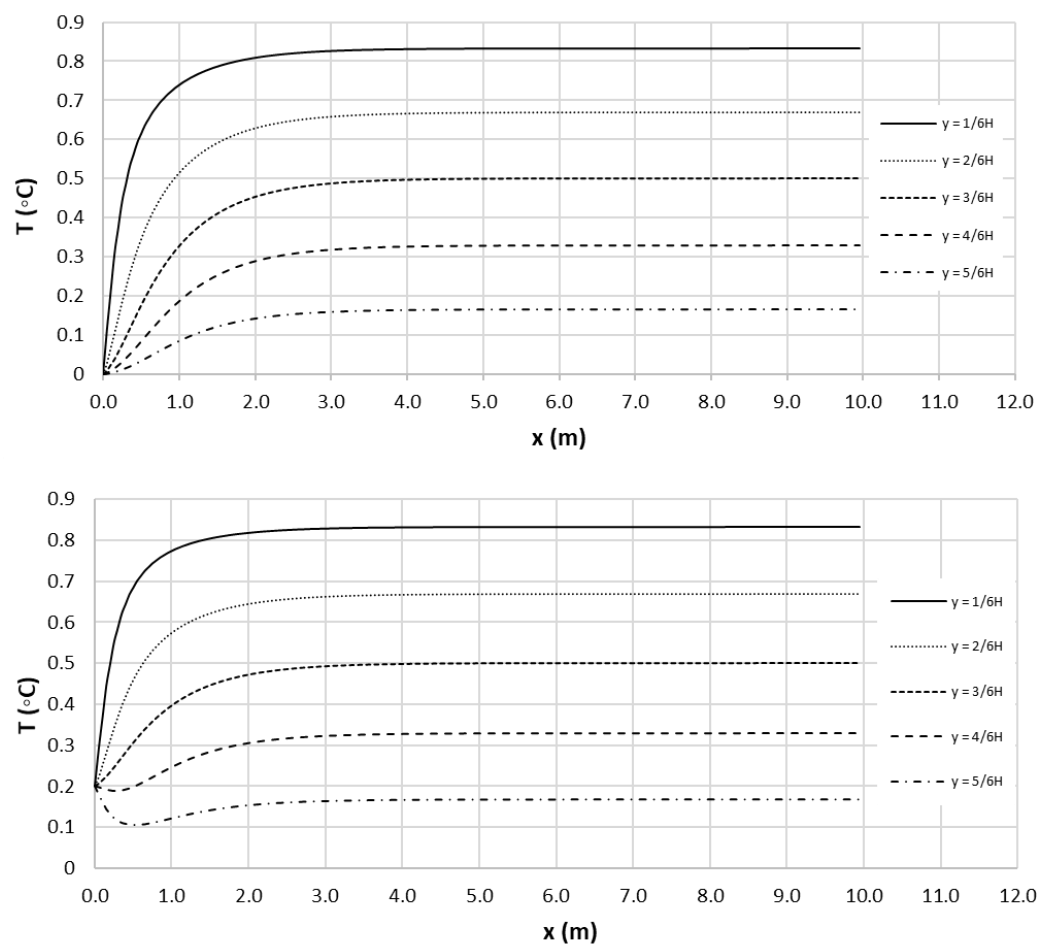$$T = 0.99 \cdot 0.5 = 0.495 \,°C, \quad l^*_{x,T \, (99\%)} = 3.3 m$$

Figure 5. Steady-state, horizontal temperature profiles of Scenarios I (**up**) and III (**down**) at $y = \frac{H}{6}, \frac{2H}{6}, \frac{3H}{6}, \frac{4H}{6}$ and $\frac{5H}{6}$.

Other criteria to define $l^*_{x,T}$ would be equally valid, for example, the distance at which the dimensionless, horizontal temperature gradient, on the line $y = H/2$, has a sufficiently small value. Figure 6 shows this component of the gradient for Scenario III in which $T_3 \in [T_1, T_2]$. In the figure, $\partial T / \partial x$ has been depicted for five regularly distributed depths, $y = \frac{H}{6}, \frac{2H}{6}, \frac{3H}{6}, \frac{4H}{6}$ and $\frac{5H}{6}$ m. The values of $l^*_{x,T}$ are, for $\partial T / \partial x = 0.02$ (1.15 °C/m), $l^*_{x,T} = 3.05$ m, while for $\partial T / \partial x = 0.01$ (0.57 °C/m), $l^*_{x,T} = 3.55$ m.
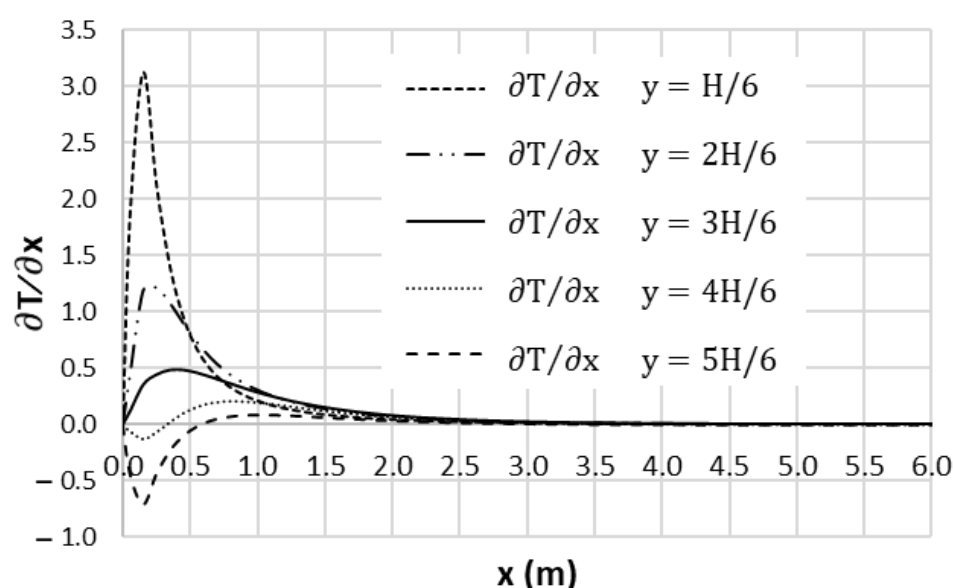
Figure 6. Values of $\partial T/\partial x$ for Scenario III at $y = \frac{H}{6}, \frac{2H}{6}, \frac{3H}{6}, \frac{4H}{6}$ and $\frac{5H}{6}$.

Finally, for scenarios where $L < l_{x,T}^*$, L itself instead of $l_{x,T}^*$ is the parameter that rules the temperature patterns of the problem.

Let us now study the influence of horizontal diffusivity against advection to justify in most real cases the hypothesis of neglecting the former. The comparison between both effects can be made through the quotient between the diffusive and advective horizontal terms of Equation (2), $k\left(\frac{\partial^2 T}{\partial x^2}\right)$ and $\rho_{e,w}c_{e,w}\left(v_{x,o}\frac{\partial T}{\partial x}\right)$, respectively. The dimensionless group that characterizes this ratio (a kind of Peclet number), the result of nondimensionalizing and averaging over the domain of the aquifer bounded by l_x^* (Bejan [27]), is

$$\pi_{\text{diff}-\text{adv}} = \frac{k}{\rho_{e,w}c_{e,w}v_{x,o}l_x^*} \tag{12}$$

Assuming the same order of magnitude for horizontal diffusion and advective effects, the order of magnitude of l_x^* (which, in contrast to $l_{x,T}^*$, does not depend on H) is given by:

$$l_x^* \sim \frac{k}{\rho_{e,w}c_{e,w}v_{x,o}} \tag{13}$$

For the fluid to reach this length, a time value of $\tau^*(s) = \frac{l_x^*}{v_{x,o}}$ will be necessary. Below this time, diffusive effects (in the region $x < l_x^*$) predominate, while above this time advective effects (in the region $x > l_x^*$) predominate.

Figure 7 shows the dependencies $l_x^* - \log(v_{x,o})$ and $\tau^* - \log(v_{x,o})$. The horizontal diffusive effect will be negligible as long as l_x^* is well below $l_{x,T}^*$ and at times when the temperature field reaches its steady-state value. For example, if $\frac{k}{\rho_{e,w}c_{e,w}} = 1\cdot10^{-6}$ m²/s and velocity is 10^{-5} m/s, typical values in many soils, from Figure 7, $l_x^* = 0.1$ m and $\tau^* = 10,000$ s are values that allow us to neglect horizontal diffusivity. However, for a velocity of 10^{-7} m/s, $l_x^* = 10$ m and $\tau^* = 1157$ days.
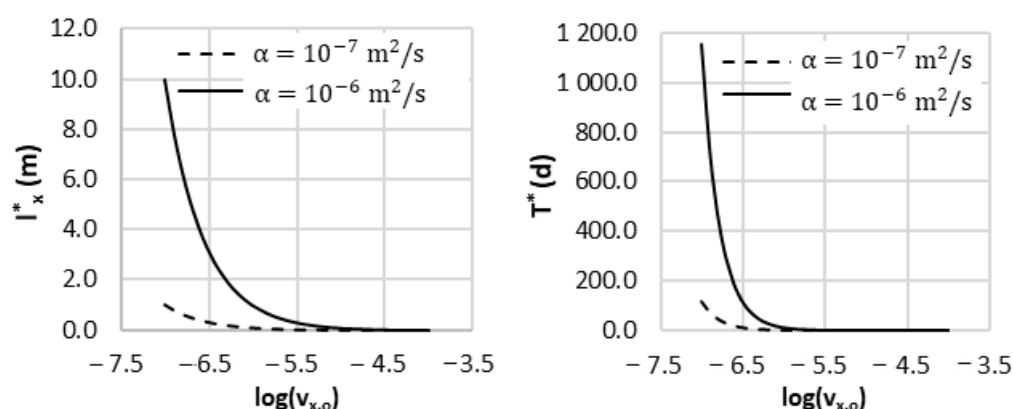
Figure 7. Dependences $l_x^* - \log(v_{x,o})$ and $\tau^* - \log(v_{x,o})$.

4. Dimensionless Characterization

This means the search of the most precise dimensionless groups on which the unknowns of interest expressed in their dimensionless form depend. An analytical expression is derived for the characteristic length since this parameter depends on a single group. In contrast, the dimensionless temperature field depends on more than one group, thus requiring numerical simulation to establish this dependence graphically.

4.1. Horizontal Characteristic Length

In this section, using pi theorem [21], the relations between the dimensionless form, the unknowns of interest and independent dimensionless groups that can be formed with the physical and geometric parameters (as well as boundary conditions) will be deduced. There are several ways to determine the dimensionless groups of a problem. The most direct is to deduce them from the dimensionless equations (Sonin [28]). In addition to a deep knowledge of the physical phenomena involved in the problem, an accurate application of dimensional analysis requires a correct choice of the dimensional basis and, in two-dimensional scenarios, the use of spatial discrimination [29].

Another more precise technique to derive the dimensionless groups is to work with the dimensionless mathematical model, that is, with governing equations and boundary conditions. It consists of defining dependent or independent variables in a dimensionless form, inserting them into the governing equations and deducing the coefficients that arise from the new equation. The independent ratios between these coefficients are the searched groups. However, to obtain the minimum and most accurate set of monomials, nondimensionalization has to be carried out in its discriminated form (discriminated dimensional analysis), which assumes that lengths, parameters and variables associated with different spatial directions have different dimensionless equations according to those directions.

The relevant variables, for the case of constant temperature at the aquifer surface that defines the steady-state temperature field in large aquifers, in which horizontal diffusivity can be neglected, are the set $\langle H, v_{x,o}, \alpha \rangle$. Introducing the normalized dimensionless variables T', x' and y' (whose value ranges are approximately [0, 1], except for the case $T_3 > \max(T_1, T_2)$ for which $T' > 1$), defined in the forms

$$T' = \frac{T - T_1}{T_2 - T_1} \tag{14}$$

$$x' = \frac{x}{l_{x,T}^*} \tag{15}$$

$$y' = \frac{y}{H} \tag{16}$$

into the governing equation $k\left(\frac{\partial^2 T}{\partial y^2}\right) - \rho_{e,w} c_{e,w}\left(v_{x,o}\frac{\partial T}{\partial x}\right) = 0$ yields the dimensionless equation:

$$k_y \frac{(T_2 - T_1)}{H^2} \frac{\partial^2 T'}{\partial y'^2} - \rho_{e,w} c_{e,w} v_{x,o} \frac{(T_2 - T_1)}{l^*_{x,T}} \frac{\partial T'}{\partial x'} = 0 \tag{17}$$

or, re-arranging coefficients,

$$\frac{l^*_{x,T} k_y}{c_{e,w} \rho_{e,w} H^2 v_{x,o}} \frac{\partial^2 T'}{\partial y'^2} - \frac{\partial T'}{\partial x'} = 0 \tag{18}$$

Therefore, the solution depends on the value of the dimensionless ratio $\frac{l^*_{x,T} k_y}{c_{e,w} \rho_{e,w} H^2 v_{x,o}} = \frac{l^*_{x,T} \alpha_m}{H^2 v_{x,o}}$ (a kind of discriminated Peclet number), which becomes a dimensionless group named $\pi_{l^*_{x,T}}$, precisely the dimensionless form of $l^*_{x,T}$. Since the equation constitutes a balance of addends, assuming that derivative terms $\frac{\partial T'}{\partial x'}$ and $\frac{\partial^2 T'}{\partial y'^2}$ can be averaged to unit by the normalized range of values of variables, the ratio $\frac{l^*_{x,T} \alpha_m}{H^2 v_{x,o}}$ must necessarily be of the order of unity. Pi theorem states that $\pi_{l^*_{x,T}} \sim 1$, or

$$l^*_{x,T} \sim \frac{H^2 v_{x,o}}{\alpha_m} \tag{19}$$

This expression can be written as an equality,

$$l^*_{x,T} = C_1 \frac{H^2 v_{x,o}}{\alpha_m} \tag{20}$$

where C_1 is a constant that can be deduced by single numerical simulation. $l^*_{x,T}$ will be defined as the distance from the left border to the point on the line $y = H/2$ where the dimensionless temperature has reached 95 (or 99)% of its steady-state value or the point for which $\partial T/\partial x = 0.01$ (or 0.02). If the dimensionless temperature has reached 99% of its steady-state value, $C_1 = 0.49$.

4.2. Dimensionless Temperature Field

In relation to the temperature field and referring firstly to the case of constant temperature at the ground surface, the existence of three boundary temperatures gives rise to the immediate appearance of a monomial that can be arbitrarily chosen as a dimensionless expression that contains these temperatures. Due to the great variety of cases that could arise in relation to values of T_1, T_2 and T_3, the construction of universal temperature curves would be a very extensive task. We will stick to the cases that, we believe, are closer to real situations in which T_3 has a value that is within interval $[T_1, T_2]$. The emergent monomial is defined in the form

$$\pi_{T_1, T_2, T_3} = \frac{T_3 - T_1}{T_2 - T_3} \tag{21}$$

so that its values, always positive, are confined to $[0, \infty]$ when $T_3 = T_1$, being infinite when $T_3 = T_2$. Defining the dimensionless temperature in the form $T'(x, y) = \frac{T - T_1}{T_2 - T_1}$, the steady-state temperature field in the region of interest $(0 \le x \le l^*_{x,T}, \ 0 \le y \le H)$, according to pi theorem, is given by

$$T'(x, y) = \frac{T - T_1}{T_2 - T_1} = f\left(\frac{x}{l^*_{x,T}}, \frac{y}{H}, \frac{T_3 - T_1}{T_2 - T_3}\right) \tag{22}$$

This expression can be particularized in horizontal and vertical profiles

$$T'(x)_{\text{vertical profile}} = \frac{T - T_1}{T_2 - T_1} = f\left(\frac{x}{l^*_{x,T}}, \frac{T_3 - T_1}{T_2 - T_3}\right) \tag{23}$$

$$T'(y)_{\text{horizontal profile}} = \frac{T - T_1}{T_2 - T_1} = f\left(\frac{y}{H}, \frac{T_3 - T_1}{T_2 - T_3}\right) \tag{24}$$

According to these expressions, the vertical profiles can be depicted by universal curves (abacus) in which each graph, which represents T' versus dimensionless depth y/H, is related with a specific value of $x/l^*_{x,T}$ (abacus parameter). Each abacus, in turn, would correspond to a different value of π_{T_1,T_2,T_3}. Similarly, the horizontal profiles would be collected in abacuses in which each graph, which represents T' versus $x/l^*_{x,T}$, would be associated with a specific value of y/H (abacus parameter), and each abacus would correspond to a value of π_{T_1,T_2,T_3}. Figure 8 represents universal surfaces (Expression (23)) of the temperature field for which π_{T_1,T_2,T_3} takes five typical values, $\pi_{T_1,T_2,T_3} = 0$ for $T_3 = T_1$, $\pi_{T_1,T_2,T_3} = 0.25$ for $T_3 = (T_2 - T_1)/5$, $\pi_{T_1,T_2,T_3} = 1$ for $T_3 = (T_2 - T_1)/2$, $\pi_{T_1,T_2,T_3} = 4$ for $T_3 = 4(T_2 - T_1)/5$ and $\pi_{T_1,T_2,T_3} = \infty$ for $T_3 = T_2$. Note that the surfaces corresponding to $\pi_{T_1,T_2,T_3} = 0.25$ and $\pi_{T_1,T_2,T_3} = 4$ can be obtained from each other by rotating 180 degrees about the horizontal axis and changing the vertical scale from $\frac{T - T_1}{T_2 - T_1}$ to $1 - \frac{T - T_1}{T_2 - T_1}$.
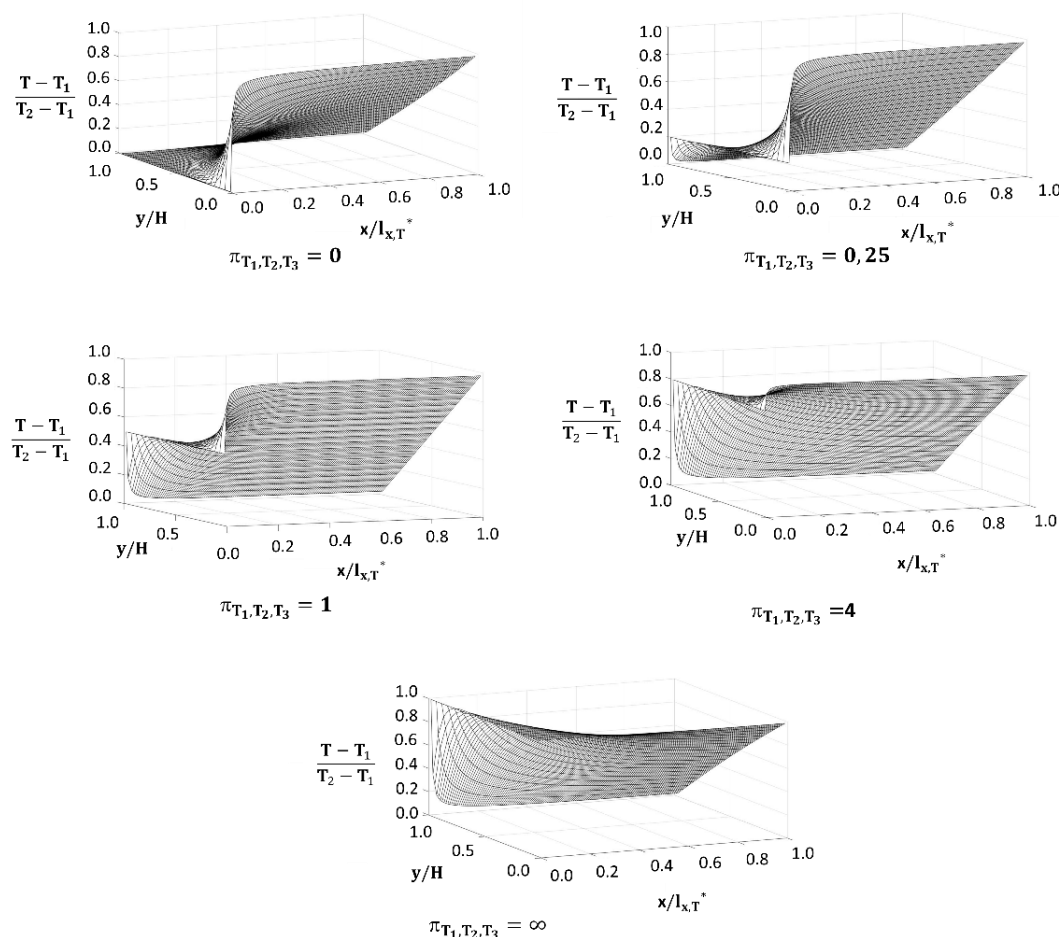

Figure 8. Universal surfaces of the temperature field (Expression (23)) for $\pi_{T_1,T_2,T_3} = 0$, $\pi_{T_1,T_2,T_3} = 0.25$, $\pi_{T_1,T_2,T_3} = 1$, $\pi_{T_1,T_2,T_3} = 4$ and $\pi_{T_1,T_2,T_3} = \infty$.

Figure 9 shows universal vertical profiles for which π_{T_1,T_2,T_3} takes five typical values $\pi_{T_1,T_2,T_3} = 0$, $\pi_{T_1,T_2,T_3} = 0.25$, $\pi_{T_1,T_2,T_3} = 1$, $\pi_{T_1,T_2,T_3} = 4$ y $\pi_{T_1,T_2,T_3} = \infty$.
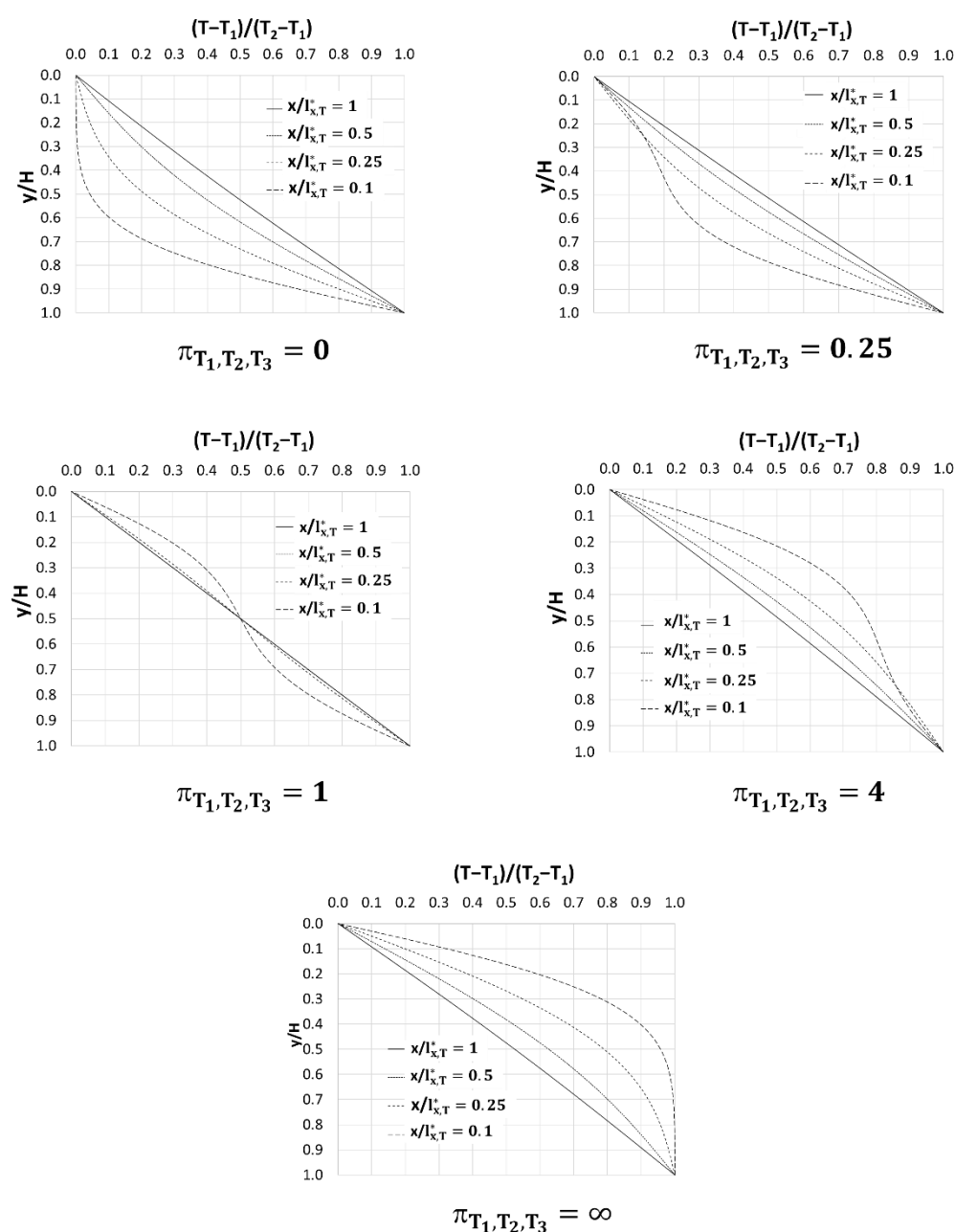
Figure 9. Universal vertical temperature–depth profiles (Expression (24)) for $\pi_{T_1,T_2,T_3} = 0$, $\pi_{T_1,T_2,T_3} = 0.25$, $\pi_{T_1,T_2,T_3} = 1$, $\pi_{T_1,T_2,T_3} = 4$ and $\pi_{T_1,T_2,T_3} = \infty$.

The use of an adequate manipulation of these abacuses allows a parametric study to be carried out to find the sensitivity of the solution to changes in the values of the physical parameters. The universal curves of Figure 9 implicitly contain this study. For example, let us define a specific scenario with known physical parameters (velocity, thermal conductivity, specific heat and height of the aquifer). For this scenario, a particular characteristic length is given by Equation (20). The profiles corresponding to each relative position $x/l_{x,T}^*$ are shown in Figure 9 (or Figure 10 for $T_3 = T_2$). If we double the thermal conductivity (retaining the value of the rest of physical parameters: velocity, specific heat and height of the aquifer), the characteristic length is reduced by half. Thus, each profile in Figure 9 moves leftwards to the curve $2(x/l_{x,T}^*)$. Therefore, the solution for the new conductivity can be inferred by direct inspection of the new set of curves.
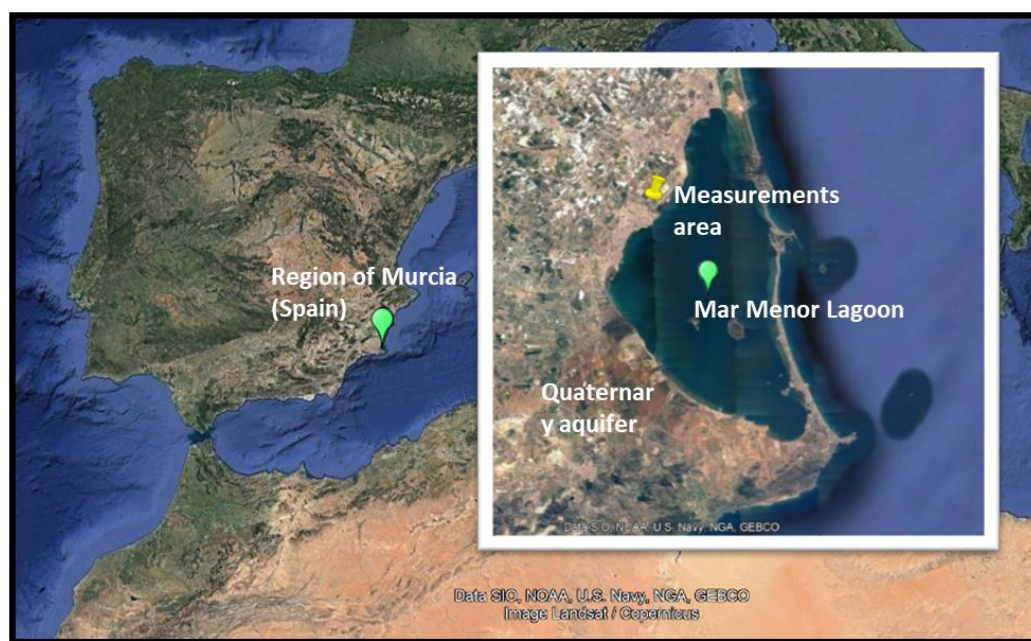
Figure 10. Location of the study area and location of measurement wells in front of Mar Menor (Google Earth Pro).

In the same way, you can infer the influence of any other parameter by looking at Equation (20). Furthermore, it is seen that certain changes in one of the parameters have similar effects from the point of view of the parametric study as certain changes in others. So, doubling the thermal conductivity has the same effect as halving the velocity, doubling the height of the aquifer has the same effect as quadrupling the thermal conductivity (or dividing the velocity by four), etc.

In summary, all the information related to the parametric study is collected in the universal solutions (abacus) of Figure 8. The shape of such curves reflects that the sensitivity of the curves to each parameter can be observed by inspection. Small characteristic lengths, which are determined either by large thermal conductivities, small specific values, small velocities and small heights or a combination of these effects, make the solution more sensitive to changes in these parameters. In contrast, large characteristic lengths determined by small thermal conductivities, large specific values, large velocities and large heights or a combination of these effects cause the curves of the abacus to close off each other.

5. Inverse Problem and Application

Firstly, we propose a protocol for the application of the inverse problem that allows estimating the water velocity flow from measurements of temperature–depth profiles. After that, an application is developed.

5.1. Inverse Problem Protocol

To estimate groundwater horizontal velocity and temperature at the left border (groundwater inlet edge), the protocol of the inverse problem described below can be applied.

Data that must be known for the application of the protocol are (a large number of measurements for locations x_1 and x_2 can be chosen):

- Depth of the aquifer: H.
- Thermal diffusivity: α_m.
- Temperatures at the surface and at the bottom of the aquifer (T_1 and T_2).
- Steady state, average temperature measured at position $(x_1, y_1 = H/4)$: $T_{x_1, H/4}$.

- Steady state, average temperature measured at position $(x_2 > x_1, y_1 = H/4)$: $T_{x_2,H/4}$.
- Steady state, average temperature measured at position $(x_1, y_1 = H/2)$: $T_{x_1,H/2}$.
- Steady state, average temperature measured at position $(x_2 > x_1, y_1 = H/2)$: $T_{x_2,H/2}$.
- Steady state, average temperature measured at position $(x_1, y_1 = 3H/4)$: $T_{x_1,3H/4}$.
- Steady state, average temperature measured at position $(x_2 > x_1, y_1 = 3H/4)$: $T_{x_2,3H/4}$.

The most unfavorable case, in which the temperature at the water inlet boundary to the domain (left boundary) is an unknown of the problem, is assumed. If temperatures T_1, T_2 and T_3 were known, we would know directly which universal abacus to use, since π_{T_1,T_2,T_3} would be known.

The steps of the protocol of the inverse problem are the following:

Step (1). Nondimensionalize temperatures $T_{x_1,H/4}$, $T_{x_1,H/2}$, $T_{x_1,3H/4}$, $T_{x_2,H/4}$ $T_{x_2,H/2}$, $T_{x_2,3H/4}$ using expressions (25) to (30):

$$T_{x_1,H/4}' = \frac{T_{x_1,H/4} - T_1}{T_2 - T_1} \tag{25}$$

$$T_{x_1,H/2}' = \frac{T_{x_1,H/2} - T_1}{T_2 - T_1} \tag{26}$$

$$T_{x_1,3H/4}' = \frac{T_{x_1,3H/4} - T_1}{T_2 - T_1} \tag{27}$$

$$T_{x_2,H/4}' = \frac{T_{x_2,H/4} - T_1}{T_2 - T_1} \tag{28}$$

$$T_{x_2,H/2}' = \frac{T_{x_2,H/2} - T_1}{T_2 - T_1} \tag{29}$$

$$T_{x_2,3H/4}' = \frac{T_{x_2,3H/4} - T_1}{T_2 - T_1} \tag{30}$$

Step (2). Find the set of universal vertical temperature–depth profiles in Figure 8 that best fit the six dimensionless temperatures. When the best-fit set of curves is found, T_3 is obtained from π_{T_1,T_2,T_3}.

Step (3). From the universal vertical temperature–depth profiles in Figure 8, $x_1' = \frac{x_1}{l_{x,T}^*}$ and $x_2' = \frac{x_2}{l_{x,T}^*}$ are obtained.

Step (4). Calculate the value of $l_{x,T}^* = \frac{x_2 - x_1}{x_2' - x_1'}$.

Step (5). Clear the value of velocity from Equation (21): $l_{x,T}^* = C_1 \frac{H^2 v_{x,o}}{\alpha_m}$.

5.2. Application in the Quaternary Aquifer–Mar Menor Interaction Scenario

To verify the protocol of the inverse problem, it will be applied to a surface water–groundwater interaction scenario. Discharges from the Quaternary aquifer (Campo de Cartagena) to the salty lagoon of the Mar Menor (SE of Spain) will be studied (Figure 10). Campo de Cartagena is a complex hydrogeological unit that occupies an approximate area of 1450 km², of which 1200 km² belongs to the Region of Murcia and the rest to the province of Alicante (Valencian Community). The Quaternary aquifer, formed by clay, silt, local conglomerate and sand facies, has an approximate thickness of between 40 and 60 m and can reach 100 m at points near the coastline [30]. The Quaternary aquifer is a very important surface aquifer from an environmental point of view, since it is the main route of discharge of groundwater and therefore of anthropogenic nutrients (mainly of agricultural origin) to the salty and coastal lagoon of Mar Menor [30–32].

Groundwater temperatures were recorded for approximately one month (26 full days from 27 January to 22 February 2022) every hour and in two wells separated by 519 m ($x_2 - x_1 = 519$ m). The closest well to the coastline was 244 m from it. From the

temperature–depth profiles measured, the average temperatures necessary for the application of the inverse problem are reflected in Table 2. On the other hand, from the bibliography [11], average thermal diffusivity is $\alpha_m = 10^{-6}$ m²/s.

Table 2. Measured temperatures in wells 1 (x_1) and 2 (x_2).

Temperature	Mean Value (°C)
T_1	17.45
T_2	22.12
$T_{x_1,H/4}$	19.93
$T_{x_1,H/2}$	21.50
$T_{x_1,3H/4}$	21.75
$T_{x_2,H/4}$	18.80
$T_{x_2,H/2}$	20.15
$T_{x_2,3H/4}$	21.15

Applying step one of the inverse problem protocol, dimensionless temperatures reflected in Table 3 are obtained.

Table 3. Dimensionless temperatures in wells 1 (x_1) and 2 (x_2).

Temperature	Value
$T_{x_1,H/4}'$	0.53
$T_{x_1,H/2}'$	0.87
$T_{x_1,3H/4}'$	0.92
$T_{x_2,H/4}'$	0.29
$T_{x_2,H/2}'$	0.58
$T_{x_2,3H/4}'$	0.79

Substituting values from Table 3 into the sets of universal curves of Figure 9, it is found that the set of curves in which dimensionless temperatures best fit are those of the abacus with parameter $\pi_{T_1,T_2,T_3} = \infty$. Therefore, $T_3 = T_2$ (see Figure 11).
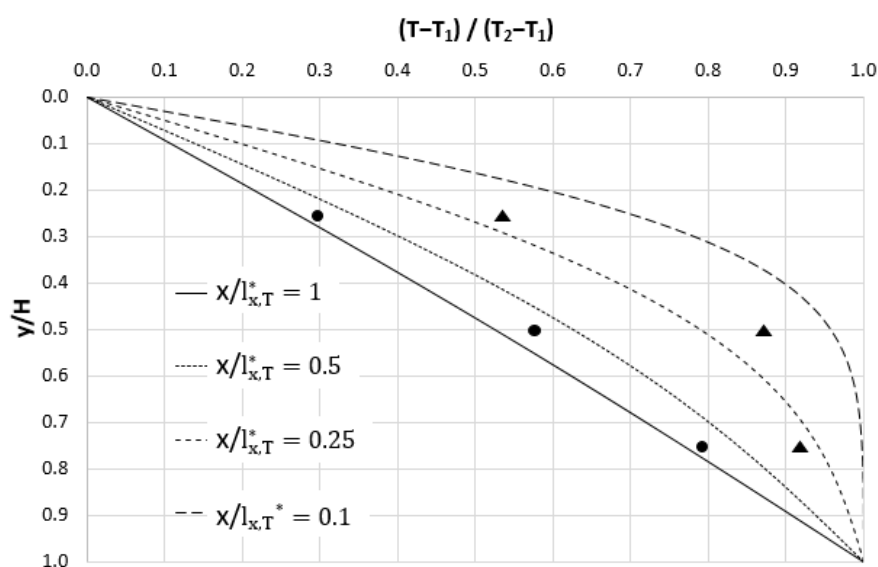

Figure 11. Application of step 2 of the inverse problem protocol. Triangles for dimensionless temperatures in well 1 (x_1) and points for dimensionless temperatures in well 2 (x_2).

From Figure 11 (applying step three), $x_1' = \frac{x_1}{l^*_{x,T}} = 0.25$ and $x_2' = \frac{x_2}{l^*_{x,T}} = 0.75$. Applying step four: $l^*_{x,T} = \frac{x_2 - x_1}{x_2' - x_1'} = \frac{519\ m}{0.5} = 1038$ m. Therefore, $x_1 = 259.20$ m and $x_2 = 778.50$ m.

Finally, the last step is to clear $v_{x,o}$ from Equation (21): $l^*_{x,T} = C_1 \frac{H^2 v_{x,o}}{\alpha_m}$.

Then, the horizontal component of groundwater discharge from the Quaternary aquifer to the salty lagoon of Mar Menor is $v_{x,o} = \frac{\alpha_m l^*_{x,T}}{H^2 C_1} = \frac{10^{-6} m^2/s \cdot 1038\ m}{(33.75\ m)^2 \cdot 0.49} = 1.86 \times 10^{-6}$ m/s.

Since it is the first time that groundwater velocity is obtained in the study area, to verify the results, the direct problem will be solved with the following input data (Table 4).

Table 4. Input data for direct problem.

T_1 (°C)	17.45
T_2 (°C)	22.12
T_3 (°C)	22.12
α_m (m²/s)	$1.00 \cdot 10^{-6}$
H (m)	33.75
L (m)	1300.00
$v_{x,o}$ (m/s)	$1.86 \cdot 10^{-6}$

The results of the direct problem as well as the error are reflected in Table 5.

Table 5. Measured temperatures in wells 1 (x_1) and 2 (x_2).

Temperature	Measured (°C)	Direct Problem (°C)	e%
$T_{x_1,H/4}$	19.93	19.31	3.21
$T_{x_1,H/2}$	21.50	20.73	3.71
$T_{x_1,3H/4}$	21.75	21.61	0.65
$T_{x_2,H/4}$	18.80	18.69	0.59
$T_{x_2,H/2}$	20.15	19.88	1.6
$T_{x_2,3H/4}$	21.15	21.02	0.62

In view of these results, it can be said that velocity is correctly estimated.

6. Contributions and Conclusions

The dimensionless groups that rule the solution patterns of the coupled 2D problem of horizontal water flow and heat transfer in aquifers under constant temperature boundary conditions have been derived. The procedure to deduce these groups starts from the dimensionless form of the governing equations which, in turn, comes from the introduction of adequate and discriminated dimensionless variables in the mathematical model. From this arises a characteristic length that defines the region in which the temperature–depth profiles depend on horizontal velocity. The simple dependence between this length and the only group on which it depends allows us to derive a precise analytical formula for this unknown. Regarding the temperature profiles, these depend on several groups: the horizontal location relative to the characteristic length, the vertical location relative to the height of the aquifer and, for the case of three temperaures at the boundary conditions, on dimensionless groups formed by these temperatures. These complex dependencies are graphically represented by abacuses using numerical simulations.

In addition, the expression that allows knowing the horizontal extension in which the diffusive and advective effects are comparable, as well as the time it would take for the fluid to travel that distance, has been obtained. This allows establishing the extent

beyond which the horizontal component of thermal diffusivity is negligible compared to the effect of advection. Furthermore, the horizontal temperature gradients are not constant at any depth but rather vary as we move away from the left border until a null value is reached.

Based on previous results, particularly on the fact that steady-state temperature profiles only depend on the relative position of the measurement point in relation to the mentioned characteristic length, an inverse problem protocol is proposed. This protocol, which is easy to apply, allows estimation of water velocity flow from the experimental measurements of six average temperatures at regular depths $y = H/4$, $y = H/2$ and $y = 3H/4$ in two different horizontal locations. The inverse problem protocol uses dimensionless temperature–depth profiles as an auxiliary tool to determine the characteristic length and subsequently the groundwater velocity. An application of the inverse problem at the Quaternary aquifer of Mar Menor lagoon (Spain) allows us to deduce the discharge of groundwater into the lagoon from agricultural activities.

Nomenclature

C_1	Constant.
C_c	Capacitor connected to central node of the elementary cell.
c_e	Volumetric heat capacity of the soil–fluid matrix ($Jm^{-3} k^{-1}$).
$c_{e,w}$	Volumetric specific heat of the water ($Jm^{-3} k^{-1}$).
f	Denotes function.
G_c	Current generator to implement flow rate.
H	Total depth of the domain (m).
$(i,j)_T$	Central node of the elementary cell.
$(i,j)_{xT}$	Central node of the left edge of each elementary cell.
$(i,j)_{yT}$	Central node of the right edge of each elementary cell.
j_c	Convection heat flux density ($Jm^{-2}s^{-1}$).
j_d	Diffusion heat flux density ($Jm^{-2}s^{-1}$).
j_s	Storage heat flux density ($Jm^{-2}s^{-1}$).
k	Thermal conductivity of the soil–fluid matrix ($cal/(sm°C)$).
L	Length of the aquifer (m).
l_x^*	Characteristic length along which the diffusive and advective effects are of the same order of magnitude (m).
$l_{x,T}^*$	Thermal characteristic length (m).
R_{xl}	Resistor arranged in direction of the x-axis in the left half of the cell.
R_{xr}	Resistor arranged in direction of the x-axis in the right half of the cell.

R_{yd}	Resistance placed in direction of the *y*-axis at the bottom of the cell.
R_{yu}	Resistance placed in direction of the *y*-axis at the top of the cell.
t	Time (s).
T	Temperature (°C).
T_1	Temperature at the soil surface (°C).
T_2	Temperature at the bottom of the aquifer (°C).
T_3	Temperature at the left border (°C).
T_{ini}	Initial soil temperature (°C).
$T'_{(x)\text{ vertical profile}}$	Vertical dimensionless temperature profile.
$T'_{(y)\text{ horizontal profile}}$	Horizontal dimensionless temperature profile.
$(T - y)$	Vertical temperature–depth profiles (°C).
$\mathbf{v}$	Water flow velocity vector (m/s).
v	Fluid velocity (m/s).
V	Denotes voltage generator.
V_f	Battery connected at central node of the bottom edge to fix a constant value temperature at the bottom of the aquifer.
V_l	Battery connected at central node of the left edge to fix a constant value temperature at the left boundary of the aquifer.
V_s	Battery connected at central node of the top boundary to fix a constant value temperature at the surface of the aquifer.
$v_{x,o}$	Horizontal flow velocity (m/s).
x, y	Spatial coordinates (m).
α	Thermal diffusivity of the soil–fluid matrix (m²/s), $\alpha = k/\rho_e c_e$.
α_m	$\alpha_m = k/\rho_{e,w} c_{e,w}$ (m²/s).
∇	Mathematical gradient operator.
$\pi_{\text{diff}-\text{adv}}$	Dimensionless group that characterizes the ratio between diffusion and advective effects over the aquifer domain l_x^*.
$\pi_{l_{x,T}^*}$	Dimensionless monomial of horizontal characteristic length.
π_{T_1,T_2,T_3}	Dimensionless temperatures monomial.
ρ_e	Wet bulk density of the soil–fluid matrix (kg/m³).
$\rho_{e,w}$	Fluid density of the water (kgm⁻³).
τ^*	Characteristic time (s).
$\|$	Absolute value.
$[]$	To denote range of values.
$\in$	Contained in.
$\sim$	Order of magnitude.
$\langle\rangle$	Symbol that encloses the list of relevant parameters of a problem.
x, y	Related to spatial directions x and y, respectively.
$\frac{H}{2}, \frac{3H}{4}$	Related to positions $\frac{H}{2}, \frac{H}{4}$ within the aquifer.
x_1, x_2	Related to positions x_1 and x_2 in the inverse problem protocol.
$(i, j)_T$	Related to central node of the elementary cell.
*	Denotes characteristic quantity.
´	Dimensionless quantity.

References

1. Lapham, W.W. *Use of Temperature Profiles Beneath Streams to Determine Rates of Vertical Ground-Water Flow and Vertical Hydraulic Conductivity*; U.S. Geological Survey Water-Supply 1989, Paper 2337; United States Geological Survey: Reston, VA, USA, 1989.
2. Animasaun, I.L.; Shah, N.A.; Wakif, A.; Mahanthesh, B.; Sivaraj, R.; Koriko, O.K. *Ratio of Momentum Diffusivity to Thermal Diffusivity: Introduction, Meta-Analysis, and Scrutinization*; Taylor & Francis: Abingdon, UK, 2022.
3. Hosseini, N.; Khoei, A.R. Modeling Fluid Flow in Fractured Porous Media with the Interfacial Conditions Between Porous Medium and Fracture. *Transp. Porous Media* **2021**, *139*, 109–129.
4. Long, G.; Xu, G. The effects of perforation erosion on practical hydraulic-fracturing applications. *SPE J.* **2017**, *22*, 645–659.

5. Yu, B. Analysis of flow in fractal porous media. *Appl. Mech. Rev.* **2008**, *61*, 050801.

6. Xiao, B.; Li, Y.; Long, G. A fractal model of power-law fluid through charged fibrous porous media by using the fractional-derivative theory. *Fractals* **2022**, *30*, 2250072-446. https://doi.org/10.1142/S0218348X22500724.

7. Suzuki, S. Percolation measurements based on heat flow through soil with special reference to paddy fields. *J. Geophys. Res.* **1960**, *65*, 2883–2885.

8. Stallman, R.W. Computation of ground-water velocity from temperature data. *USGS Water Supply Pap.* **1963**, *1544*, 36–46.

9. Bredehoeft, J.D.; Papadopulos, I.S. Rates of vertical groundwater movement estimated from the Earth's thermal profile. *Water Resour. Res.* **1965**, *1*, 325–328.

10. Ziagos, J.P.; Blackwell, D.D. A model for the transient temperature effects of horizontal fluid flow in geothermal systems. *J. Volcanol. Geotherm. Res.* **1986**, *27*, 371–397.

11. Taniguchi, M. Evaluation of vertical groundwater fluxes and thermal properties of aquifers based on transient temperature-depth profiles. *Water Resour. Res.* **1993**, *29*, 2021–2026.

12. Lu, N.; Ge, S. Effect of horizontal heat and fluid flow on the vertical temperature distribution in a semiconfining layer. *Water Resour. Res.* **1996**, *32*, 1449–1453.

13. Holzbecher, E. Inversion of temperature time series from near-surface porous sediments. *J. Geophys. Eng.* **2005**, *2*, 343–348.

14. Kulongoski, J.T.; Izbicki, J.A. Simulation of fluid, heat transport to estimate desert stream infiltration. *Groundwater* **2008**, *46*, 462–474.

15. Duque, C.; Müller, D.; Sebok, E.; Haider, K.; Engesgaard, P. Estimating groundwater discharge to surface waters using heat as a tracer in low flux environments: The role of thermal conductivity. *Hydrol. Process.* **2016**, *30*, 383–395.

16. McCord, J.; Reiter, M.; Phillips, F. Heat-flow data suggest large ground-water fluxes through Fruitland coals of the northern San Juan basin, Colorado-New Mexico. *Geology* **1992**, *20*, 419–422.

17. Constantz, J. Heat as a tracer to determine streambed water exchanges. *Water Resour. Res.* **2008**, *44*. https://doi.org/10.1029/2008wr006996.

18. Szymkiewicz, A.; Tisler, W.; Burzyński, K. Examples of numerical simulations of two-dimensional unsaturated flow with VS2DI code using different interblock conductivity averaging schemes. *Geologos* **2015**, *21*, 161–167.

19. Cartwright, K. Redistribution of geothermal heat by a shallow aquifer. *Geol. Soc. Am. Bull.* **1971**, *82*, 3197–3200.

20. Manteca, I.A.; Alcaraz, M.; Trigueros, E.; Alhama, F. Dimensionless characterization of salt intrusion benchmark scenarios in anisotropic media. *Appl. Math. Comput.* **2014**, *247*, 1173–1182.

21. Buckingham, E. On physically similar systems; illustrations of the use of dimensional equations. *Phys. Rev.* **1914**, *4*, 345.

22. Lecampion, B.; Detournay, E. An implicit algorithm for the propagation of a hydraulic fracture with a fluid lag. *Comput. Methods Appl. Mech. Eng.* **2007**, *196*, 4863–4880.

23. Sánchez-Pérez, J.F.; Alhama, I. Simultaneous determination of initial porosity and diffusivity of water-saturated reinforced concrete subject to chloride penetration by inverse problem. *Constr. Build. Mater.* **2020**, *259*, 120412.

24. Alhama, I.; García-Ros, G.; Icardi, M. Non-Stationary Contaminant Plumes in the Advective-Diffusive Regime. *Mathematics* **2021**, *9*, 725.

25. González-Fernández, C.F.; Alhama, F. *Heat Transfer and the Network Simulation Method*; Horno, J., Ed.; Transworld Research Network: Trivandrum, India, 2001

26. Sánchez Pérez, J.F.; Conesa, M.; Alhama, I.; Alhama, F.; Cánovas, M. Searching fundamental information in ordinary differential equations. Nondimensionalization technique. *PLoS ONE* **2017**, *12*, e0185477.

27. Bejan, A. *Convection Heat Transfer*; John Wiley & Sons: Hoboken, NJ, USA, 2013.

28. Sonin, A.A. A generalization of the Π-theorem and dimensional analysis. *Proc. Natl. Acad. Sci. USA* **2004**, *101*, 8525–8526.

29. Madrid, C.N.; Alhama, F. Discrimination: A fundamental and necessary extension of classical dimensional analysis theory. *Int. Commun. Heat Mass Transf.* **2006**, *33*, 287–294.

30. Rey, J.; Martínez, J.; Barberá, G.G.; García-Aróstegui, J.L.; García-Pintado, J.; Martínez-Vicente, D. Geophysical characterization of the complex dynamics of groundwater and seawater exchange in a highly stressed aquifer system linked to a coastal lagoon (SE Spain). *Environ. Earth Sci.* **2013**, *70*, 2271–2282.

31. Del Ebro, C.H. Informe de Sostenibilidad Ambiental del Plan Especial de Actuación en Situaciones de Alerta y Eventual Sequía en la Cuenca Hidrográfica del Ebro. MIMAM. Zaragoza. 2007. Available online: http://vishub.org/officedocs/7088.pdf (accessed on 10 June 2022).

32. Garcia-Pintado, J.; Martínez-Mena, M.; Barberá, G.G.; Albaladejo, J.; Castillo, V.M. Anthropogenic nutrient sources and loads from a Mediterranean catchment into a coastal lagoon: Mar Menor, Spain. *Sci. Total Environ.* **2007**, *373*, 220–239.